Forced G1-phase reduction alters mode of division, neuron number, and laminar phenotype in the cerebral cortex

Louis-Jan Pilaz[a,b], Dorothée Patti[a,b], Guillaume Marcy[a,b], Edouard Ollier[a,b], Sabina Pfister[c], Rodney J. Douglas[c], Marion Betizeau[a,b], Elodie Gautier[a,b], Veronique Cortay[a,b], Nathalie Doerflinger[a,b], Henry Kennedy[a,b], and Colette Dehay[a,b,1]

[a]Stem Cell and Brain Research Institute, Institut National de la Santé et de la Recherche Médicale, U846, 18 Avenue Doyen Lepine, 69500 Bron France; [b]Université de Lyon, Université Lyon I, 69003 Lyon, France; and [c]Institute of Neuroinformatics, Swiss Federal Institute of Technology (University ETH), 8092 Zurich, Switzerland

Edited by Jon H. Kaas, Vanderbilt University, Nashville, TN, and approved October 21, 2009 (received for review August 31, 2009)

The link between cortical precursors G1 duration (TG1) and their mode of division remains a major unresolved issue of potential importance for regulating corticogenesis. Here, we induced a 25% reduction in TG1 in mouse cortical precursors via forced expression of cyclin D1 and cyclin E1. We found that in utero electroporation-mediated gene transfer transfects a cohort of synchronously cycling precursors, necessitating alternative methods of measuring cell-cycle phases to those classical used. TG1 reduction promotes cell-cycle reentry at the expense of differentiation and increases the self-renewal capacities of Pax6 precursors as well as of Tbr2 basal precursors (BPs). A population level analysis reveals sequential and lineage-specific effects, showing that TG1 reduction: (*i*) promotes Pax6 self-renewing proliferative divisions before promoting divisions wherein Pax6 precursors generate Tbr2 BPs and (*ii*) promotes self-renewing proliferative divisions of Tbr2 precursors at the expense of neurogenesis, thus leading to an amplification of the BPs pool in the subventricular zone and the dispersed mitotic compartment of the intermediate zone. These results point to the G1 mode of division relationship as an essential control mechanism of corticogenesis. This is further supported by long-term studies showing that TG1 reduction results in cytoarchitectural modifications including supernumerary supragranular neuron production. Modeling confirms that the TG1-induced changes in neuron production and laminar fate are mediated via the changes in the mode of division. These findings also have implications for understanding the mechanisms that have contributed to brain enlargement and complexity during evolution.

basal progenitor | cell-cycle | corticogenesis

Cortical areas are characterized by their cytoarchitecture, an expression of the morphology and density of their constituent neurons. Areal differences in neuron number and phenotype are distinguishing features both within and across species (1, 2). The developmental processes that specify the number of neurons and their laminar fate are therefore instrumental in specifying cortical cytoarchitecture. Neuron number in layers and areas correlate with changes in the rate of neuron production, largely determined by the balance between cell-cycle reentry and exit (3, 4). Proliferative division generates two progenitors that re-enter the cell-cycle, whereas differentiative division gives rise to at least one daughter cell that undergoes differentiation. An open question is how the decision between proliferative versus differentiative division is made (5).

Key observations suggest a concerted regulation of TG1 and mode of division. During mouse corticogenesis, a progressive increase in rates of neuron production, is accompanied by increasing frequencies of differentiative divisions, and a slowing down of TG1 (6). Proliferative divisions are characterized by short TG1 and differentiative divisions by long TG1 (3, 7–9). G1 represents a critical phase during cell-cycle progression, where precursors are competent to respond to extracellular cues, influencing commitment to a further round of cell division or withdrawal from the cell cycle and embarking on a differentiation pathway (10). These observations and others (11, 12) led to the hypothesis that TG1 could be an integral part of a cellular mechanism regulating the mode of division (13, 14).

However, there are two studies where the G1 phase regulation has been modified in cortical neuroblasts and that failed to reveal a link between TG1 and mode of division. Mitsuhashi et al. (15) reported that transient $p27^{Kip1}$ overexpression in VZ precursors induces TG1 lengthening without altering the balance between proliferative and differentiative divisions. Tarui et al. (16) claimed that overexpression of $p27^{Kip1}$ increased neurogenic differentiative divisions without altering TG1. These reports as well as other studies failing to report or detect a correlation between the changes in TG1 and mode of division during corticogenesis in normal (17) and mutant mice (18–20) leave this important issue still unresolved.

In corticogenesis the G1 mode of division relationship raises specific issues with respect to the heterogeneity of the precursor populations, because they are known to exhibit different modes of division (13, 21). In the mouse, the ventricular zone (VZ) contains predominantly Pax6-expressing precursors that have extensive proliferation capacities, and the subventricular zone (SVZ) is populated by the BPs, which undergo predominantly symmetric differentiative neurogenic divisions (22, 23).

Results

A major requirement of this study is the selective modification of TG1 of cortical precursors in vivo. The progression through G1 phase is driven by the sequential kinase activity of cyclin D/cdk4 and cyclin E/cdk2 (24). However, cyclin D has been reported to also exert cell-cycle independent functions on migration and differentiation (25, 26) and cdk4 and cdk2 can trigger other signaling pathways (27, 28). Cyclin E1 is known to have less pleiotropic effects. Because both cyclin E1 and cyclin D1 have been shown to be rate limiting for G1/S transition (29), our strategy has been to overexpress cyclin E1 and cyclin D1 and to report on both sets of results. To do this we used in utero electroporation, a highly efficient method of DNA plasmid

Author contributions: C.D. designed research; L.-J.P., D.P., G.M., E.O., S.P., R.J.D., M.B., E.G., V.C., and N.D. performed research; L.-J.P., D.P., G.M., M.B., V.C., H.K., and C.D. analyzed data; and L.-J.P., H.K., and C.D. wrote the paper.

The authors declare no conflict of interest.

This article is a PNAS Direct Submission.

Freely available online through the PNAS open access option.

[1]To whom correspondence should be addressed. E-mail: colette.dehay@inserm.fr.

This article contains supporting information online at www.pnas.org/cgi/content/full/0909894106/DCSupplemental.

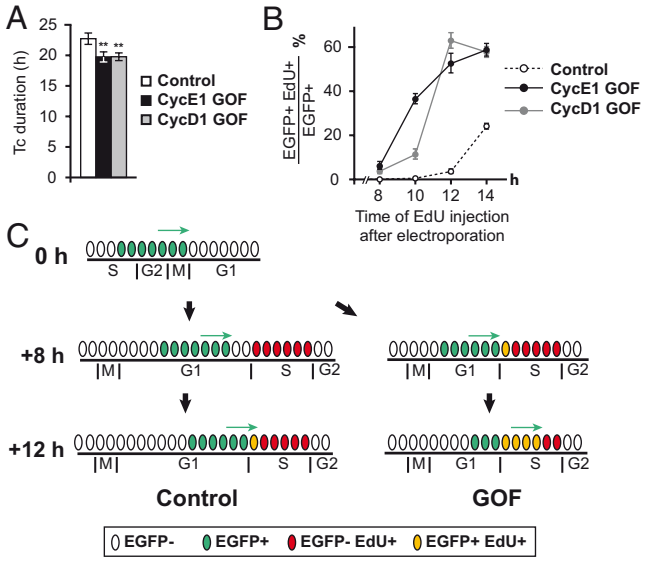

Fig. 1. Overexpression of cyclin E1 and cyclin D1 influence cell-cycle characteristics of cortical precursors. (*A*) Cell-cycle duration (Tc) of control and GOF precursors measured by time-lapse videorecording, on E14.5 organotypic slices, 24 h after electroporation. Overexpression of cyclin E1 and cyclin D1 leads to a significant shortening of Tc (22.8 h in control; range: 15–28 h, $n = 16$) vs. 19.75 h in GOF precursors (GOF cyclin E1: range: 13–23 h, $n = 13$; GOF cyclin D1: range: 13–22 h, $n = 25$). Unpaired t test: cyclin E1 GOF: $P = 0.0024$; cyclin D1 GOF: $P = 0.0075$. (*B*) TG1 in GOF and control transfected precursors. A small proportion of EdU+/EGFP+ cells are detected in both GOF conditions, 8 h after electroporation, whereas the first EDU+/EGFP+ precursors (3.3%) are detected only 12 h after electoporation in control precursors. (*C*) Diagram: Electroporation transfects a cohort of cells in late S, G2/M phases (cells in green). The EGFP+ cohort progresses through G1 phase at different rates between control and GOF conditions. Only GOF precursors have reached S phase 8 h after electroporation.

delivery into the precursors lining the VZ, so as to target presumptive somatosensory cortical precursors.

We coelectroporated human cyclin E1 [known to interact with the mouse cell-cycle machinery, (30)] and murine cyclin D1 with EGFP in E15 embryonic brains. Gain of function (GOF) of human cyclin E1 and murine cyclin D1 will be referred to as cyclin E1 GOF and cyclin D1 GOF, respectively. Rates of coelectroporation were >95% (31). Protein expression levels of cyclin E1 and cyclin D1 were measured by using confocal quantification of immunofluorescent labeling (3). Significantly higher levels of cyclin E1 and cyclin D1 were observed in GOF cells and their progeny than in control cells (EGFP electroporated) (Fig. S1 *A* and *B*).

We found that electroporation-mediated transfection in the VZ triggers overexpression in a synchronized cohort of cycling precursors (see *SI Results*, Fig. S1 *C–E*, and Movie S1), thereby precluding the use of BrdU cumulative labeling and percentage of labeled mitotic figures as valid techniques to measure the cell-cycle parameters of the EGFP expressing precursors (Figs. S1 and S2 *A–C*). The influence of cyclin D1 and cyclin E1 overexpression on cell-cycle kinetics was first assessed ex vivo. After in utero electroporation targeting the dorsomedial cortex at E14.5, 2-photon time-lapse imaging was performed on organotypic slices at E15.5. The time period between two successive mitosis corresponds to the cell-cycle duration Tc. We observed a mean Tc of 23 h in control EGFP+ cells and 19.75 h in both cyclin E1 GOF and cyclin D1 GOF cells, indicating a 15% reduction of Tc in GOF precursors (Fig. 1*A*). Using a double S phase-labeling procedure in vivo, we then show a significant reduction of Tc minus Ts (Ts: S phase duration) in GOF precursors compared to control (Fig. S2*D*). To directly measure TG1 in vivo in the electroporated population, we performed EdU pulse injections 8, 10, and 12 h after in utero electroporation at E15. Ten hours after electroporation, <0.05% EGFP+ cells in the controls had incorporated EdU, this contrasted with the cyclin E1 and cyclin D1 GOF populations where 38 and 10% of cells were double-labeled, respectively (Fig. 1*B*). Twelve hours after electroporation, the proportion of EdU+ EGFP+ cells had greatly increased in the GOF population, reaching 50% (cyclin E1 GOF) and 60% (cyclin D1 GOF) and contrasting with <5% of EdU+ cells in the control population, indicating that control cells had just begun to enter S phase. Because EGFP is not expressed in those cells that were electroporated during the G1 phase, the first EGFP+ cells to incorporate EdU are those cells that were in M phase at the time of electroporation (Fig. 1*C*). This experimental procedure, which allows the measurement of the minimum TG1 value, indicates that TG1 is nearly 4 h shorter in the GOF populations compared to controls. Importantly, similar TG1 reductions were observed in both Pax6+ and Tbr2+ GOF precursors (Fig. S2 *E–G*). Shorter TG1 in cyclin E1 and cyclin D1 overexpressing precursors was confirmed by the lower frequency of cells showing a punctuate Ki67 staining, characteristic of cycling cells in G1/S phases (17) (Fig. S3*A*).

Altering the Balance Between Proliferative and Differentiative Divisions. The consequences of the forced TG1 reduction on the proliferative behavior of cortical precursors was first examined in dissociated cultures over a 3-day period. E15 precursors were transfected via lipofection and the size of individual clones resulting from the transfection of a single precursor were measured. The average number of cells per clone and the clonal sizes distribution show significant differences between cyclin E1 and cyclin D1 GOF precursors and controls (Fig. 2*A* and *B*). Whereas the average clone size was three cells (median size: 1.95) in controls, with >50% of clones being composed of one or two cells, the average clone size was four cells (median size: 2.94 for cyclin E1 GOF and 2.96 for cyclin D1 GOF) in GOF conditions with a high proportion of clones being composed of more than five cells.

Ki67 is expressed during all phases of the cell cycle in most cells, which makes it an appropriate growth fraction marker (32). Variations in the proportions of Ki67+ cells in a precursor population are therefore indicative of variations in the proportions of cell-cycle reentry (proliferative divisions) versus cell-cycle exit (differentiative divisions). Ki67 immunostaining performed 3 days after transfection showed that the proportion of cycling precursors is significantly increased in the GOF clones compared to controls. This indicates a higher fraction of cell-cycle reentry in GOF clones, consistent with cyclin E1 and cyclin D1 overexpression leading to an increase in the proportion of proliferative divisions (Fig. 2 *A* and *C*).

In vivo, cyclin E1 and cyclin D1 GOF led to a significant increase in the proportions of Ki67 expressing precursors in the GZ 24 and 48 h after electroporation, confirming cell-cycle reentry at the expense of differentiation (Fig. 2*D*). Conversely, down-regulation of cyclin D1 and cyclin E1 via transfection of targeted siRNAs led to a decrease in the proportions of cell-cycle reentry (Fig. S3*B*). This shows that forced TG1 reduction promotes proliferative divisions of cortical precursors at the expense of neurogenesis.

Consequences on the Total Precursor Pool Size. The increase in cell-cycle reentry induced by cyclin D1 and cyclin E1 GOF led to an amplification of the precursor pool, as revealed by a significant increase in the thickness of the GZ in the electroporated region compared with the equivalent nonelectroporated region (Fig. S4 *A–C* and Table S1). This increase is detectable

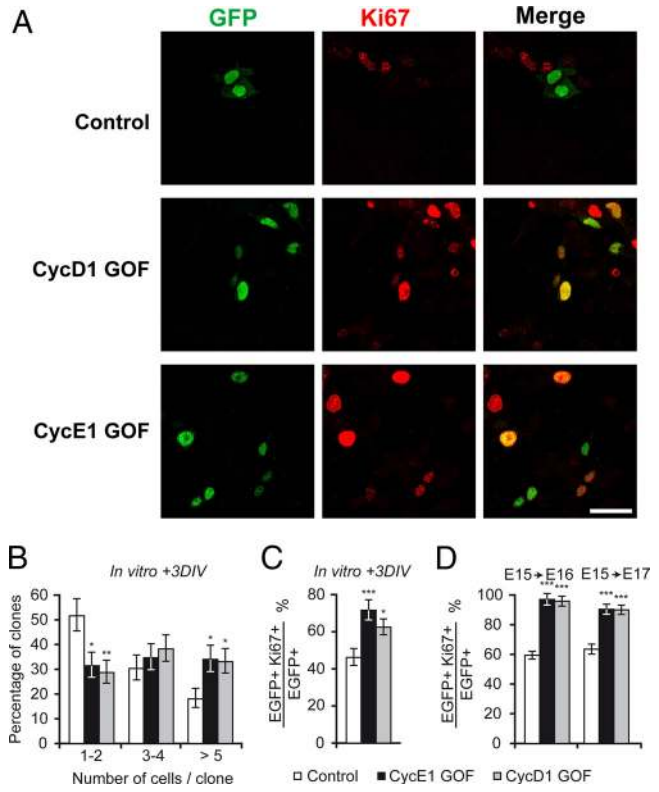

Fig. 2. Proliferative status of overexpressing cyclin E1 and cyclin D1 precursors. (*A*) Microphotographs showing clone size and Ki67 expression in dissociated cortical precursors, 3 days after in vitro lipofection at E15. (Scale bars, 40 μm.) (*B*) Clones sizes in control and GOF precursors: dissociated cultures, 3 days after in vitro lipofection at E15. GLM analysis: clones 1–2 cyclin E1 GOF: $P = 0.015$; clone 1–2 cyclin D1 GOF: $P = 0.0039$; clone >5 cyclin E1 GOF: $P = 0.017$; clone >5 cyclin D1 GOF: $P = 0.020$. (*C*) Percentage of cycling cells in control and GOF transfected populations and their progeny in dissociated cultures, as shown by Ki67 expression. GLM analysis: cyclin E1 GOF: $P = 0.00042$; cyclin D1 GOF: $P = 0.011$. (*D*) Percentage of cycling cells in the transfected populations and their progeny, as shown by Ki67 expression. Measurements were made in the GZ in vivo. GLM analysis: E15–E16: cyclin E1 GOF: $P < 0.001$; E15–E16: cyclin D1 GOF: $P < 0.001$; E15–E17: cyclin E1 GOF: $P < 0.001$; E15–E17: cyclin D1 GOF: $P < 0.001$.

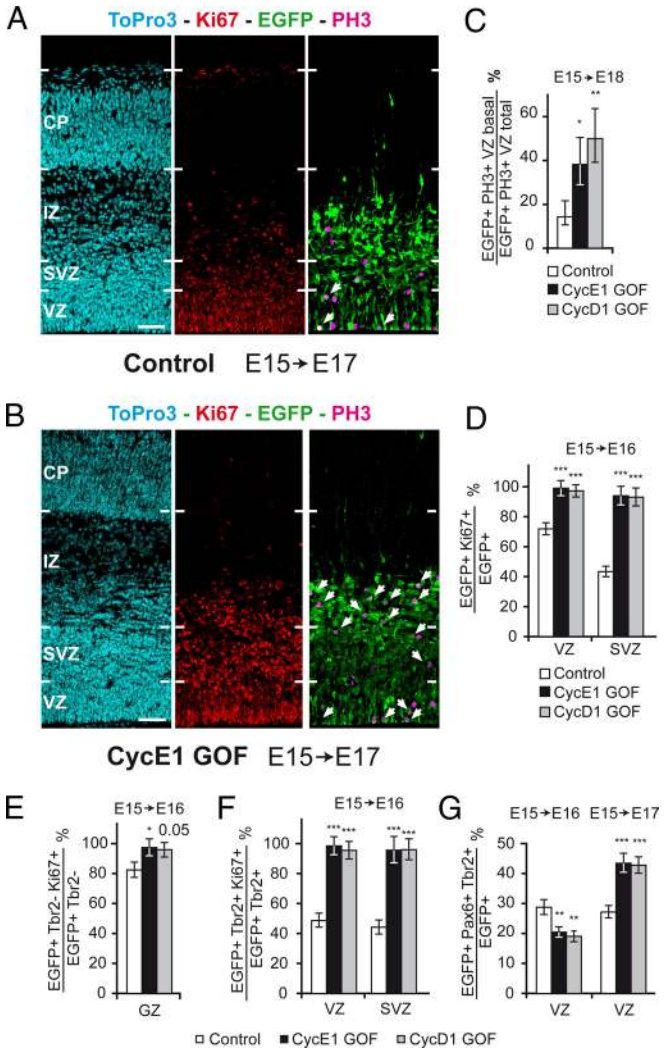

Fig. 3. Consequence of GOF on precursor pools. (*A* and *B*) Confocal microphotographs of coronal sections showing Ki67 and PH3 expressing cells in the electoporated regions of E17 brains, after electroporation at E15. Arrows indicate EGFP+ PH3+ mitotic cells. (Scale bars, 50 μm.) High power views of Z projections to show colocalisation of PH3 and EGFP are shown in Fig. S5 *B–D*. (*C*) Higher proportions of basal mitosis figures in the VZ in GOF conditions than in control conditions. GLM analysis: cyclin E1 GOF: $P = 0.027$; E15–E18 cyclin D1 GOF: $P = 0.0092$. (*D*) Percentage of cycling cells in the transfected populations and their progeny, as shown by Ki67 expression, in vivo. GLM analysis: VZ cyclin E1 GOF: $P < 0.001$; VZ cyclin D1 GOF: $P < 0.001$; SVZ cyclin E1 GOF: $P < 0.001$; SVZ cyclin D1 GOF: $P < 0.001$. (*E*) Percentage of Tbr2- cycling cells in the transfected populations and their progeny, as shown by Ki67 expression, in vivo. GLM analysis: GZ cyclin E1 GOF: $P = 0.049$; GZ cyclin D1 GOF: $P = 0.054$. (*F*) Percentage of Tbr2+ cycling cells in the Tbr2+ transfected populations and their progeny, as shown by Ki67 expression in vivo. GLM analysis: VZ cyclin E1 GOF: $P < 0.001$; VZ cyclin D1 GOF: $P < 0.001$; SVZ cyclin E1 GOF: $P < 0.001$; SVZ cyclin D1 GOF: $P < 0.001$. (*G*) Percentage of Tbr2+ Pax6+ cells in the transfected population and their progeny in the VZ. GLM Analysis: E15–E16 cyclin E1 GOF: $P = 0.0048$; E15–E16 cyclin D1 GOF: $P = 0.0013$; E15–E17 cyclin E1 GOF: $P < 0.001$; E15–E17 cyclin D1 GOF: $P < 0.001$.

48 h after electroporation and persists 72 h after electroporation (Fig. S4*A*). We have quantified the increase in the number of precursors by counting the number of Ki67+ cells in a 100-μm wide column of E17 cortex after GOF electroporation at E15. Counts were compared on coronal sections between the electroporated region and the homologous region of the control hemisphere. The results show a significant 25% increase in the number of Ki67+ precursors (Fig. S4*D*). The sparse zone of Ki67+ proliferative cells located in the bottom part of the IZ (33–36) makes a major contribution (23%, Fig. S4 *E* and *F*) to the increase in the total number of proliferative cells per column of cortex under GOF conditions.

Sequential and Lineage-Specific Consequences on Pax6- and Tbr2-Expressing Precursors. We investigated the impact of TG1 shortening on apically dividing Pax6 and Tbr2 BPs precursor pools. PH3 immunolabeling performed 72 h after electroporation at E15 reveal a significant increase in the numbers of precursors in the VZ undergoing basal mitosis in GOF precursors compared to controls (Fig. 3*C*). Measurements of the absolute thickness of VZ and SVZ made in strictly corresponding loci between control and GOF electroporated regions showed a significant increase (30 to 50%) in the thicknesss of the SVZ at 48 and 72 h (Fig. S4 *B* and *C* and Table S1). By contrast, no significant variation in the thickness of the VZ was observed (Fig. S4*C* and Table S1). The increase in basal mitosis in cyclin E1 and cyclin D1 GOF conditions is likely to be responsible for the increase in thickness of the SVZ.

We analyzed independently and sequentially the consequences of cyclin E1 and cyclin D1 GOF on the proliferation of VZ and SVZ precursors by monitoring the percentage of Ki67+

cells. In the VZ, there is a 26% increase in Ki67+, 24 h after electroporation in GOF conditions and a 117% increase in the SVZ (Fig. 3 *A*, *B*, and *D* and Fig. S5*A*). These increases are due to the increase in the proportions of Ki67+ cells in both the Pax6 (Fig. 3*E*) and Tbr2 populations (Fig. 3*F*).

To explore the impact of TG1 reduction on the fate of daughter cells generated by proliferative divisions, we quantified the proportions of (*i*) Pax6+/Tbr2−, (*ii*) Tbr2+/Pax6− (mature BPs), and (*iii*) Pax6+/Tbr2+ in the VZ and SVZ, 24 and 48 h after electroporation. Pax6+/Tbr2+ cells correspond to newborn Tbr2+, where Pax6 expression has not yet been down-regulated (22). Twenty-four hours after electroporation, we observed a significant increase in the proportion of Pax6+ cells in the VZ accompanied by a significant reduction of Tbr2+ precursors (Fig. S6*A*). This indicates that, at this stage TG1 shortening promotes self-renewing proliferative divisions of Pax6 precursors. This is further supported by the decreased proportions of Pax6+/Tbr2+ in the VZ (Fig. 3*G*, left histograms). Forty-eight hours after electroporation, TG1 reduction resulted in a statistically significant decrease of Pax6+ proportions and a concomitant increase in Tbr2+ in the VZ (Fig. S6*B*). Conversely, down-regulation of cyclinD1 and cyclinE1 led to an increase in the proportions of Pax6+ precursors and a corollary decrease in the proportion of Tbr2+ precursors in the VZ, while no change was observed in the SVZ (Fig. S6*B*). The observed increase in Tbr2 proportions in the VZ at 48 h is in agreement with the shift from apical to basal mitosis observed in GOF precursors (Fig. 3 *A–C* and Fig. S5). We observed a significant increase in the proportions of Pax6+/Tbr2+ precursors in the GOF electroporated populations compared to controls (Fig. 3*G*, right histograms), indicating a shift toward the production of Tbr2 precursors in the Pax6 progeny. This effect is reversed by down-regulation of cyclin D1 and cyclin E1 (Fig. S6 *C* and *E*).

At the population level, forced expression of cyclin D1 and cyclin E1 influence VZ precursors by first promoting self-renewing proliferative divisions of Pax6+ cells. In a second step, Pax6 precursors proliferative divisions shift toward an increased generation of Tbr2+ BPs. Overexpression of cyclin E1 and cyclin D1 influences precursor fate in a similar fashion. At both stages, the proportion of post-mitotic neurons (Pax6-Tbr2- cells) is statistically reduced in the GOF population (Fig. S6*D*), confirming an increase in proliferative at the expense of differentiative neurogenic divisions. Conversely, down-regulation of cyclin D1 and cyclin E1 increases the proportion of post-mitotic cells in the VZ (Pax6-Tbr2-) (Fig. S6*F*).

These results, together with the observation showing similar rates of cell death in control and GOF conditions (Fig. S6 *G–I*), suggest that there could be two processes contributing to the increase of the SVZ precursor pool observed at 48 and 72 h after electroporation. In a first instance, a transient amplification of the Pax6 precursor pool (possibly via increased rates of symmetric self-renewing proliferative divisions), followed by an increase in proliferative divisions of Pax6 precursors generating Tbr2 precursors that leave the VZ for the SVZ. Subsequently, a drastic increase in proliferation of Tbr2 precursors in both VZ and SVZ: the magnitude of the increase in Ki67 proportions in the Tbr2 populations is high (110%) and approximately equivalent in the VZ and the SVZ (Fig. 3*F*).

Changes in Laminar Fate and Cytoarchitecture in the Postnatal Cortex. Because EGFP expression is retained for several weeks, we have been able to examine the consequences of cyclin E1 and cyclin D1 overexpression on neuron production and fate. First, we examined the laminar distribution of EGFP expressing neurons in area 3 (somatosensory cortex) and the adjacent area 4 at postnatal day 15 (P15), after completion of migration of cortical neurons. Control EGFP-expressing neurons are largely (90%)

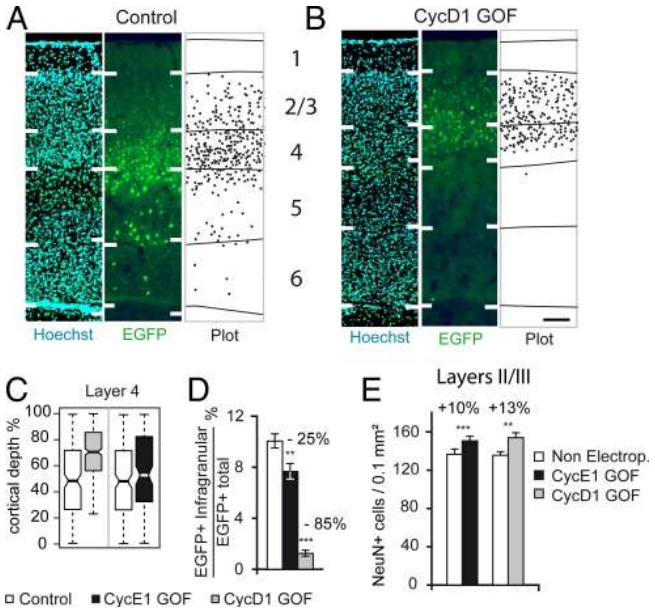

Fig. 4. Laminar phenotype of post-mitotic neurons generated by the transfected precursors, 2 weeks after birth, under control and GOF conditions. (*A* and *B*) Photomicrographs of a transect of Hoechst and EGFP stained coronal section in area 3 showing the limits of plots of the distribution of EGFP expressing neurons born from control (*A*) and GOF (*B*) precursors. (Scale bar, 100 μm.) (*C*) Box plot analysis of the radial distribution of layer 4 EGFP neurons, born from control and GOF precursors in area 3. Individual box indicates mid 50th percentile range of individual distance neuron measurements. Whiskers, 10th to 90th percentiles; horizontal bold line, mean. (*D*) EGFP labeled neurons located in the infragranular layers, in control and GOF conditions. GLM analysis: cyclin E1 GOF: $P = 0.0054$; cyclin D1 GOF: $P < 0.001$. (*E*) Variations in neuron density in the supragranular layers of the electroporated region compared to control, at P15. Paired *t* test: cyclin E1 GOF: $P < 0.001$; cyclin D1 GOF: $P < 0.001$.

located in the supragranular layers (including layer 4), with scattered cells in the infragranular layers (Fig. 4*A* and *B* and Fig. S7 *A* and *B*). A significant reduction in the proportion of infragranular located neurons was observed in the GOF progeny (10% in control vs. 7.5 and 1.5% in cyclin E1 and cyclin D1, respectively) (Fig. 4*D*). In layer 4, GOF progeny neurons were restricted to the upper half of the layer (Fig. 4 *A* and *B* and Fig. S7 *A* and *B*), whereas control EGFP progeny neurons occupy the full width of the layer. A box plot analysis revealed that the laminar depth was statistically different in control and GOF progenies in layer 4 (Fig. 4*C* and Fig. S7*C*). These results indicate that after TG1 shortening, neurons exit the cell-cycle later during corticogenesis and produce neurons of the phenotype predicted by their birthdate (37, 38).

The impact of TG1 modifications on rates of neuron production was measured via neuron counts in control and electroporated regions in supra- and infragranular layers in the P15 cortex. This revealed a significant 10% increase in the neuron density in layer 3 of the GOF electroporated region compared to control (Fig. 4*E*). Neuron density was identical in layer 6B and lower although not significantly different in layer 5 of the GOF electroporated region compared to control (Fig. S7*D*). TG1 shortening from E15 to E17 modified rates of neuron production and cytoarchitectonic features, resulting in a significant increase in supragranular layer neuron density.

Mathematical Modeling of the Consequences of Shortening G1 and Increasing Cell-Cycle Reentry on Neuron Production and Laminar Fate. Modeling the effects of GOF on TG1 and cell-cycle reentry from E15 to E17 provides predictions of changes in neuron number in a laminar specific fashion (see *SI Results*). The predicted increase

in neuron numbers is 26.94% in layers 2/3 and a global increase of 4.16%, contrasting with a predicted drop in layer 5 by −16.84% (Fig. S8 *A–C*). The drop in layer 5 is because the E15 precursors that are progenitors of layer 5 are induced to undergo further rounds of proliferative divisions in GOF conditions. In agreement with the timetable of cortical layer production in area 3 (37, 38), layer 6B neuron numbers are not affected by GOF induced changes in cell-cycle parameters occurring after E15 (Fig. S8*D*). The agreement between the modeled data and the experimental observations is good, the latter showing a 10% increase in density of supragranular layer neurons and a modest drop in layer 5 neuron density in GOF conditions compared to control (Fig. 4*E* and Figs. S7*D* and S8 *B* and *C*). The modeled data also predicts the changes in the laminar location of the progeny of the GOF precursors in good agreement with the experimental data (Fig. 4*D*), (reduction infragranular data: 1.24%, model: 3.27%) (Fig. 4*D* and Fig. S4*E*) compared to neurons born from control precursors (data: 10%, model: 16.19%) (Fig. 4*D* and Fig. S4*E*). These changes conform to the relationship between a neuron birth date and its laminar phenotype (39).

Discussion

Because recent studies have reported cell-cycle independent roles of certain cdkis on migration and differentiation (40), selective TG1 lenghtening via overexpression of G1/S inhibitors is not appropriate. Therefore, proof of a causal link between TG1-phase progression and mode of division requires the demonstration that selectively reducing TG1 leads to an increase in proliferative divisions. A recent study investigated this issue in younger cortical precursors (41). However, the results are difficult to interpret concerning the role of TG1 on mode of division because of the inappropriate techniques used to measure cell-cycle phases duration in the synchronously cycling cohort of electroporated precursors.

Work in embryonic stem cells have led to the hypothesis that shortening of TG1 might shield stem cells from signals that induce differentiation (42, 43). A prolonged TG1 could be a characteristic feature of differentiative divisions, facilitating the integration of extrinsic signals that influence cell fate and/or allowing an unequally inherited cell-fate determining factor(s) to act over a sufficient time period (7).

Differential Effect on Pax6 and Tbr2 Precursors. The mechanisms regulating the generation of BPs from Pax6 precursors are currently incompletely understood (20, 44, 45). The present results, by showing alterations in Pax6 progeny fate subsequent to TG1 modification, point to these mechanisms being also related to cell-cycle regulation. Because cyclin E1 has been shown to promote asymmetric proliferative divisions, independently of its role on the G1/S transition, in thoracic neuroblasts of the *Drosophila* (46), one can also hypothesize that its forced expression could be responsible for an increase in asymmetric (Pax6 -> Pax6 +Tbr2) proliferative divisions .

The rates of cell-cycle reentry were increased with a much greater magnitude in the Tbr2 population (+80%) (Fig. 3*F*) compared to the Pax6 population (Fig. 3*E*). This differential effect could be related to the fact that Pax6 precursors have greater self-renewal/proliferative abilities than do Tbr2 cells (47). These differential effects of TG1 shortening on Pax6 and Tbr2 precursors have structural consequences on the germinal compartments. Whereas in GOF conditions, the thickness of the VZ, predominantly populated by Pax6 expressing precursors (Fig. S9), is not modified, the thickness of the SVZ is greatly increased (+100%). (Note that the measurements of putative changes in the tangential extent of the VZ cannot be assessed because this will be biased by the size of the electoporated territory, which is subjected to individual experimental variations that cannot be precisely controlled).

Impact on Laminar Fate and Cytoarchitecture. Long-term survival times revealed that the modifications in TG1 and mode of division increase neuron number in layers 2 and 3 and modify the laminar fate of the progeny neurons. Theoretical modeling returns numerical values that agree with experimental observations (Fig. S8), indicating that the observed changes in cytoarchitecture and laminar fate are the consequences of the modifications in cell-cycle parameters, and more specifically of the increase in proliferative divisions given that TG1 reduction alone is not able to recover the observed effects (Fig. S8*F*).

The present experimental and modeling data converge to show that TG1 influences the mode of division, which in turn is the major player in determining the size of the precursor pool and neuron production. This means that the fine-tuning of the G1 phase of the cell cycle is the primary parameter that orchestrates the exquisitely ordered neuron production during corticogenesis. This raises questions regarding mechanisms controlling corticogenesis in primate where Tc and TG1 are much longer than in the rodent (3, 48).

The differential effects of G1 reduction on BPs and Pax6 expressing precursors suggest cell cycle-related evolutionary mechanisms that may have contributed to the selective enlargement of the supragranular layers in primate brain (5, 49–53). The increase in proliferative divisions, leading to a transient amplification of the BPs pool, captures a major feature of primate corticogenesis. Remarkably, this "primatization" of the mouse GZ translates in to an enlarged supragranular layer compartment, a hallmark of the primate brain.

Materials and Methods

Animals. OF1 mice were kept under a 12-h light/12-h dark schedule. E1 is the day of vaginal plug detection, and P0 is the date of birth. Animal protocols were approved by the University of Lyon.

In Utero Electroporation. A xylasin/ketamin mix was used to anesthetize pregnant OF1 mice. Briefly, the uterine horns were exposed, and plasmids (2–3 μL) with Fast Green (0.01 mg/mL; Sigma) were pressure microinjected through the uterine wall into the lateral ventricles of embryos via pulled glassed capillaries (1–2 μg/mL total plasmid concentration, 2.4 μM siRNA constructs). Five pulses of current (50 ms on/1,000 ms off) were delivered (voltages 60 V) by using a pair of tweezertrodes (BTX Harvard Apparatus, diameter 1 cm) pinching the whole body of each embryo through the uterine wall. The electrodes were placed with the anode on the injected hemisphere to target the dorsomedial cortex. In coelectroporation, ratios of DNA plasmid were 2 for EGFP plasmid and 3 for cyclinE1and cyclinD1.

Plasmids and siRNA. Full-length cDNAs encoding mouse cyclin D1 (NM_007631) and human variant 2 of cyclin E1 (NM_057182) were inserted into the unique *Bst*XI site of the pHpCAG expression plasmid (54) to generate pHpCAG-hCyclE and pHpCAG-mCyclD1, respectively. pCAGGS-IRES-GFP vector was generously provided by J. Briscoe (National Institute for Medical Research London, U.K.), where a [cDNA]-nlsIRES-EGFP cassette is under the control of an CMV-enhancer and a chicken beta-actin promoter (40). All constructs were verified by sequencing. The following siRNAs were predesigned by Ambion (ref. 160056): 5′-GGCAAAUGUGGCCGUGUUUtt-3′ (sense strand) and 5′-AAACACGGCCACAUUUGCCtt-3′ for mouse cyclin E1, and (ref. 160053): 5′-CGAUUUCAUCGAACACUUCtt-3′ (sense strand) and 5′-GAAGUGUUCGAUGAAAUCGtg-3′ (antisense strand) for mouse cyclin D1.

Preparation of brain sections, Immunofluorescence and antibodies, counting of cell types, organotypic slice culture and bi-photon imaging, confocal analysis, BrdU and EdU labeling, statistical analysis, and mathematical modeling were as described in the *SI Results*.

ACKNOWLEDGMENTS. We thank Dr. Ken Knoblauch for invaluable guidance for the statistical analysis; Pascale Giroud and Anne-Cécile Boulay for help with results analysis; Murielle Séon, Nikola Kolomitre, and Marco Valebenito for animal care; Camille Lamy, Pierre Misery, and Jennifer Beneyton for technical help; and Veronique Vezoli and Maud Brittain for administrative help and grant management. This work was supported by Agence Nationale de la Recherche Grants 06-NEUR-010–01 and European Union Grants EU FP6–2005 IST-1583 (Daisy) and EU FP7–216593 (Seco).

1. Herculano-Houzel S, Collins CE, Wong P, Kaas JH, Lent R (2008) The basic nonuniformity of the cerebral cortex. *Proc Natl Acad Sci USA* 105:12593–12598.
2. Rockel AJ, Hiorns RW, Powell TP (1980) The basic uniformity in structure of the neocortex. *Brain* 103:221–244.
3. Lukaszewicz A, et al. (2005) G1 phase regulation, area-specific cell cycle control, and cytoarchitectonics in the primate cortex. *Neuron* 47:353–364.
4. Polleux F, Dehay C, Moraillon B, Kennedy H (1997) Regulation of neuroblast cell-cycle kinetics plays a crucial role in the generation of unique features of neocortical areas. *J Neurosci* 17:7763–7783.
5. Rakic P (1995) A small step for the cell, a giant leap for mankind: A hypothesis of neocortical expansion during evolution. *Trends Neurosci* 18:383–388.
6. Takahashi T, Nowakowski RS, Caviness VSJ (1995) The cell cycle of the pseudostratified ventricular epithelium of the embryonic cerebral wall. *J Neurosci* 15:6046–6057.
7. Calegari F, Huttner WB (2003) An inhibition of cyclin-dependent kinases that lengthens, but does not arrest, neuroepithelial cell cycle induces premature neurogenesis. *J Cell Sci* 116:4947–4955.
8. Dehay C, Savatier P, Cortay V, Kennedy H (2001) Cell-cycle kinetics of neocortical precursors are influenced by embryonic thalamic axons. *J Neurosci* 21:201–214.
9. Lukaszewicz A, Savatier P, Cortay V, Kennedy H, Dehay C (2002) Contrasting effects of basic fibroblast growth factor and neurotrophin 3 on cell cycle kinetics of mouse cortical stem cells. *J Neurosci* 22:6610–6622.
10. Zetterberg A, Larsson O, Wiman KG (1995) What is the restriction point? *Curr Opin Cell Biol* 7:835–842.
11. Iacopetti P, et al. (1999) Expression of the antiproliferative gene TIS21 at the onset of neurogenesis identifies single neuroepithelial cells that switch from proliferative to neuron-generating division. *Proc Natl Acad Sci USA* 95:4639–4644.
12. Georgopoulou N, et al. (2006) BM88 is a dual function molecule inducing cell cycle exit and neuronal differentiation of neuroblastoma cells via cyclin D1 down-regulation and retinoblastoma protein hypophosphorylation. *J Biol Chem* 281:33606–33620.
13. Gotz M, Huttner WB (2005) The cell biology of neurogenesis. *Nat Rev Mol Cell Biol* 6:777–788.
14. Dehay C, Kennedy H (2007) Cell-cycle control and cortical development. *Nat Rev Neurosci* 8:438–450.
15. Mitsuhashi T, et al. (2001) Overexpression of p27Kip1 lengthens the G1 phase in a mouse model that targets inducible gene expression to central nervous system progenitor cells. *Proc Natl Acad Sci USA* 98:6435–6440.
16. Tarui T, et al. (2005) Overexpression of p27 Kip 1, probability of cell cycle exit, and laminar destination of neocortical neurons. *Cereb Cortex* 15:1343–1355.
17. Miyata T, et al. (2004) Asymmetric production of surface-dividing and non-surface dividing cortical progenitor cells. *Development* 131:3133–3145.
18. Cappello S, et al. (2006) The Rho-GTPase cdc42 regulates neural progenitor fate at the apical surface. *Nat Neurosci* 9:1099–1107.
19. Cubelos B, et al. (2008) Cux-2 controls the proliferation of neuronal intermediate precursors of the cortical subventricular zone. *Cereb Cortex* 18:1758–1770.
20. Sahara S, O'Leary DD (2009) Fgf10 regulates transition period of cortical stem cell differentiation to radial glia controlling generation of neurons and basal progenitors. *Neuron* 63:48–62.
21. Pinto L, et al. (2008) Prospective isolation of functionally distinct radial glial subtypes–lineage and transcriptome analysis. *Mol Cell Neurosci* 38:15–42.
22. Englund C, et al. (2005) Pax6, Tbr2, and Tbr1 are expressed sequentially by radial glia, intermediate progenitor cells, and postmitotic neurons in developing neocortex. *J Neurosci* 25:247–251.
23. Noctor SC, Martinez-Cerdeno V, Ivic L, Kriegstein AR (2004) Cortical neurons arise in symmetric and asymmetric division zones and migrate through specific phases. *Nat Neurosci* 7:136–144.
24. Sherr CJ, Roberts JM (2004) Living with or without cyclins and cyclin-dependent kinases. *Genes Dev* 18:2699–2711.
25. Coqueret O (2002) Linking cyclins to transcriptional control. *Gene* 299:35–55.
26. Li Z, Wang C, Prendergast GC, Pestell RG (2006) Cyclin D1 functions in cell migration. *Cell Cycle* 5:2440–2442.
27. Faber AC, Chiles TC (2007) Inhibition of cyclin-dependent kinase-2 induces apoptosis in human diffuse large B-cell lymphomas. *Cell Cycle* 6:2982–2989.
28. Ovcharenko D, Kelnar K, Johnson C, Leng N, Brown D (2007) Genome-scale microRNA and small interfering RNA screens identify small RNA modulators of TRAIL-induced apoptosis pathway. *Cancer Res* 67:10782–10788.
29. Resnitzky D, Reed SI (1995) Different roles for cyclins D1 and E in regulation of the G1-to-S transition. *Mol Cell Biol* 150:3463–3469.
30. Geng Y, et al. (1999) Rescue of cyclin D1 deficiency by knockin cyclin E. *Cell* 97:767–777.
31. Rosen GD, et al. (2007) Disruption of neuronal migration by RNAi of Dyx1c1 results in neocortical and hippocampal malformations. *Cereb Cortex* 17:2562–2572.
32. Scholzen T, Gerdes J (2000) The Ki-67 protein: From the known and the unknown. *J Cell Physiol* 182:311–322.
33. Noctor SC, Martinez-Cerdeno V, Kriegstein AR (2008) Distinct behaviors of neural stem and progenitor cells underlie cortical neurogenesis. *J Comp Neurol* 508:28–44.
34. Sturrock RR, Smart IH (1980) A morphological study of the mouse subependymal layer from embryonic life to old age. *J Anat* 130:391–415.
35. Tabata H, Kanatani S, Nakajima K (2009) Differences of migratory behavior between direct progeny of apical progenitors and basal progenitors in the developing cerebral cortex. *Cereb Cortex*, 19:2092–2105.
36. Konno D, et al. (2008) Neuroepithelial progenitors undergo LGN-dependent planar divisions to maintain self-renewability during mammalian neurogenesis. *Nat Cell Biol* 10:93–101.
37. Polleux F, Dehay C, Kennedy H (1998) Neurogenesis and commitment of corticospinal neurons in reeler. *J Neurosci* 18:9910–9923.
38. Polleux F, Dehay C, Kennedy H (1997) The timetable of laminar neurogenesis contributes to the specification of cortical areas in mouse isocortex. *J Comp Neurol* 385:95–116.
39. Polleux F, Dehay C, Goffinet A, Kennedy H (2001) Pre- and post-mitotic events contribute to the progressive acquisition of area-specific connectional fate in the neocortex. *Cereb Cortex* 11:1027–1039.
40. Nguyen L, et al. (2006) p27kip1 independently promotes neuronal differentiation and migration in the cerebral cortex. *Genes Dev* 20:1511–1524.
41. Lange C, Huttner WB, Calegari F (2009) Cdk4/cyclinD1 overexpression in neural stem cells shortens G1, delays neurogenesis, and promotes the generation and expansion of basal progenitors. *Cell Stem Cell* 5:320–331.
42. Fluckiger AC, et al. (2006) Cell cycle features of primate embryonic stem cells. *Stem Cells* 24:547–556.
43. Burdon T, Smith A, Savatier P (2002) Signalling, cell cycle and pluripotency in embryonic stem cells. *Trends Cell Biol* 12:432–438.
44. Sansom SN, et al. (2009) The level of the transcription factor Pax6 is essential for controlling the balance between neural stem cell self-renewal and neurogenesis. *PLoS Genet* 5:e1000511.
45. Pinto L, et al. (2009) AP2gamma regulates basal progenitor fate in a region- and layer-specific manner in the developing cortex. *Nat Neurosci* 12:1229–1237.
46. Chia W, Somers WG, Wang H (2008) *Drosophila* neuroblast asymmetric divisions: Cell cycle regulators, asymmetric protein localization, and tumorigenesis. *J Cell Biol* 180:267–272.
47. Huttner WB, Kosodo Y (2005) Symmetric versus asymmetric cell division during neurogenesis in the developing vertebrate central nervous system. *Curr Opin Cell Biol* 17:648–657.
48. Kornack DR, Rakic P (1998) Changes in cell-cycle kinetics during the development and evolution of primate neocortex. *Proc Natl Acad Sci USA* 95:1242–1246.
49. Kriegstein A, Noctor S, Martinez-Cerdeno V (2006) Patterns of neural stem and progenitor cell division may underlie evolutionary cortical expansion. *Nat Rev Neurosci* 7:883–890.
50. Smart IH, Dehay C, Giroud P, Berland M, Kennedy H (2002) Unique morphological features of the proliferative zones and postmitotic compartments of the neural epithelium giving rise to striate and extrastriate cortex in the monkey. *Cereb Cortex* 12:37–53.
51. Fish JL, Dehay C, Kennedy H, Huttner WB (2008) Making bigger brains-the evolution of neural-progenitor-cell division. *J Cell Sci* 121:2783–2793.
52. Molnar Z, et al. (2006) Comparative aspects of cerebral cortical development. *Eur J Neurosci* 23:921–934.
53. Lukaszewicz A, et al. (2006) The concerted modulation of proliferation and migration contributes to the specification of the cytoarchitecture and dimensions of cortical areas. *Cereb Cortex* 16:i26–34.
54. Niwa H, Burdon T, Chambers I, Smith A (1998) Self-renewal of pluripotent embryonic stem cells is mediated via activation of STAT3. *Genes Dev* 12:2048–2060.